Published in final edited form as:
*ACS Med Chem Lett*. 2011 January 1; 2(4): 285–288. doi:10.1021/ml1002844.

# PET Imaging and Biodistribution of Silicon Quantum Dots in Mice

**Chuqiao Tu**[†], **Xuchu Ma**[‡], **Adrian House**[†], **Susan M. Kauzlarich**[*,‡], and **Angelique Y. Louie**[*,†]

[†] Department of Biomedical Engineering, University of California, Davis, One Shields Avenue, Davis, California 95616, United States

[‡] Department of Chemistry, University of California, Davis, One Shields Avenue, Davis, California 95616, United States

## Abstract

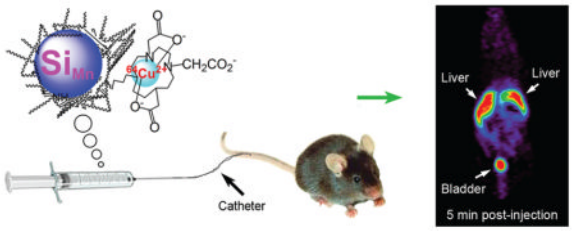


Investigation of nanomaterial disposition and fate in the body is critical before such material can be translated into clinical application. Herein a new macrocyclic ligand–$^{64}Cu^{2+}$ complex was synthesized and used to label dextran-coated silicon quantum dots (QD), with an average hydrodynamic diameter of 15.1 ± 7.6 nm. The chelate showed exceptional stability, demonstrated by no loss radiolabel under a ligand competition reaction with EDTA. The QDs' biodistribution in mice was quantitatively evaluated by *in vivo* positron emission tomography (PET) imaging and *ex vivo* gamma counting. Results showed that they were excreted via renal filtration shortly postinjection and also accumulated in the liver.

### Keywords

Biodistribution; positron emission tomography; imaging; silicon; quantum dot

Over the past decade, quantum dots (QDs) have been touted as promising agents for *in vivo* biomedical imaging due to their desirable properties of high quantum yield, resistance to photobleaching, narrow emission peak, and tunable emission wavelength.[1–3] Investigation of nanomaterial disposition and fate in the body, i.e. biodistribution and plasma clearance, is critical before such material can be translated into clinical application. The biodistribution of group II–VI QDs has been investigated in rodents via both fluorescence and radioactivity-



[*]Corresponding Author: S.M.K., smkauzlarich@ucdavis.edu; A.Y.L., aylouie@ucdavis.edu.

**Author Contributions**

C.Q.T. developed Si QDs coating synthesis, executed $^{64}Cu$ radiolabeling and *in vivo* PET imaging, and wrote manuscript. X.C.M. synthesized Si cores. A.H. handled animals. S.M.K and A.Y.L. conceived of design, syntheses, experiments and edited manuscript.

Supporting Information. Synthetic procedures and characterization of compounds **1**–**4** and nanoparticles **5** and **6**, details of the stability measurements of $^{64}Cu$ labeled dextran $Si_{Mn}$ QDs, and *in vivo* PET imaging and *ex vivo* gamma counting procedures. This material is available free of charge via the Internet at http://pubs.acs.org.

based techniques.[1,4–6] However, to date, such studies have not been reported for recently emerged, fluorescent silicon QDs, which are expected to be an ideal candidate for many biological applications because of their biocompatibility.[7–11]

Taking advantage of the QD's intrinsic luminescence properties, optical imaging techniques can be used to investigate QDs *in vitro* and offer the benefits of noninvasiveness, high sensitivity, and relatively low cost. However, for *in vivo* use, tissue absorption and scattering of light impair excitation of QDs in deeper lying tissues, and the fluorescence signal detected from deeper structures is significantly attenuated as a function of tissue depth, which makes optical tracking and quantification of QDs in living systems difficult.[6] For example, there are studies showing that current fluorescence imaging systems significantly underestimate QD mass amounts in living animals, especially in deep tissues, and therefore are not robust enough to accurately measure *in vivo* biodistribution.[4,12]

Positron emission tomography (PET) is a noninvasive, highly sensitive nuclear imaging technique that can produce three-dimensional images.[13–15] We have used PET to track the biodistribution of a wide array of imaging probes. The results demonstrated that this noninvasive imaging technique is capable of providing a robust and reliable measure of *in vivo* probe distribution.[16–18] PET has been employed to study biodistribution in living animals of group II–VI CdSe QDs radiolabeled with a positron-emitting tracer.[4,19] Herein, we report the evaluation of Si QDs biodistribution in mice using $^{64}$Cu labeled Si QDs for both *in vivo* PET imaging and gamma counting of *ex vivo* tissues.

Silicon QDs were synthesized from the precursor sodium silicide through a solution-phase reduction, as previously reported, except that $Si_{Mn}$ QDs ($Si_{Mn}$ QDs = 1% manganese doped Si QDs) were coated with neutral dextran instead of anionic dextran sulfate.[11] The dextran sulfate coated Si QDs are targeted to macrophages while the dextran coated Si QDs are nonspecific nanoparticles. That is, they do not interact specifically with any type of cells and therefore report the clearance of Si QDs from the body mainly based on the particle size.[11,20] DOTA (1,4,7,10-tetraazacyclododecane-1,4,7,10-tetraacetic acid) is a frequently used ligand for chelation of $^{64}$Cu ion that forms a complex of high thermodynamic stability (DOTA-Cu log $K$ = 20–28).[4,21–24] However, in practice we found that attachment of commercially available *p*-SCN-Bn-DOTA to the particles using traditional bioconjugation methods was synthetically difficult, probably due to the steric hindrance caused by the short and rigid arm of SCN-Bn.[17] Therefore, we synthesized a new bifunctional DO3A (1,4,7,10-tetraazacyclododecane-1,4,7-triacetic acid) derivative **4** that has a more flexible functional arm for chelation of $^{64}$Cu. The conjugation of ligand **4** with the dextran coating of $Si_{Mn}$ QDs was realized by polarity inversion of dextran hydroxyl groups.

The synthetic route for ligand **4** is shown in Scheme 1. Di-*tert*-butyl dicarbonate and 3-bromopropylamine hydrobromide were stirred in methanol in the presence of triethylamine to afford compound **1** in 79% yield. After cyclen was monoalkylated with **1**, the resultant compound **2** was further alkylated with 3 equiv of *tert*-butyl bromoacetate to produce compound **3**.[25,26] Compound **3** was hydrolyzed with trifluoroacetic acid in dichloromethane to give the free ligand **4** as an adduct of trifluoroacetic acid to free base, which was confirmed by $^{1}$H and $^{13}$C NMR and the strong absorption at −74.25 ppm in $^{19}$F NMR of **4**.

The polarity of dextran was partially inverted by esterification with 4-nitrophenyl chloroformate and 4-(dimethylamino)pyridine (DMAP) (catalyst) in DMSO/pyridine.[27] The following nucleophilic addition–elimination reactions of polar, partially inverted dextran with propylamine capped $Si_{Mn}$ QDs and ligand **4** generated DO3A conjugated, dextran coated $Si_{Mn}$ QDs **5**,[11] as shown in Scheme 2. The average hydrodynamic diameter of the purified particle **5** was 15.1 ± 7.6 nm. Particle **5** contained 1.5% silicon. Its emission peak

was at 440 nm and the intensity of emission was maximal for excitation at 360 nm, similar to our previous results for the unconjugated particles.[11] The results support that particle **5** is dextran coated silicon QDs, which is important because the dextran alone can form different sizes of nanoparticles.[28] DO3A conjugated $Si_{Mn}$ QDs **5** were metalated with $^{64}CuCl_2$ in pH 5.5 acetate buffer solution followed by the extraction of possible uncoordinated free copper ions by applying excess ethylenediaminetetraacetic acid (EDTA). After purification by centrifuge filtration, the radiolabeling yield was found to be 78%.

To confirm that $^{64}Cu$ ions remain attached to the QDs **6** during imaging and verify that distribution is not due to free dissociated copper, the kinetic stability of QDs **6**-$^{64}Cu$ was tested by subjecting QDs **6**-$^{64}Cu$ to a competitive ligand exchange with EDTA, which is known to have a high affinity for Cu (log $K_{Cu\text{-}EDTA}$ = 18.7),[29] over the 48-h time period. Figure 1 shows that, over time, the QDs **6**-$^{64}Cu$ in pH 5.5 sodium acetate–acetic acid buffer solution do not lose radiolabel, confirming the exceptional stability of the chelator.

The clearance of $Si_{Mn}$ QDs **6** from the blood circulation is rapid, as shown in Figure 2. By 2 min post tail-vein injection, 95.7%ID/g (percentage of injected dose per gram blood or tissue) has already been cleared out from the bloodstream. The rapid clearance continued until 10 min postinjection, when <2.5%ID/g was left in the bloodstream. Thereafter, the clearance slowed and ~1.5%ID/g remained in the blood 120 min postinjection. The fast blood clearance of $Si_{Mn}$ QDs **6** is similar to that of polyethylene glycol coated CdSe QDs (12 or 21 nm, respectively) measured by PET imaging and gamma counting in mice, which were also cleared in minutes,[4] but differs from reports of polymer-coated QDs or dextran-coated iron oxide nanoparticles measured by fluorescence imaging, which had similar hydrodynamic diameters to $Si_{Mn}$ QDs **6** but much longer blood circulation times of up to a few hours.[1,6,16]

The concentrations of particles radiolabeled with positron-emitting tracer can be determined semiquantitatively from the PET images and used to analyze the biodistribution of $Si_{Mn}$ QDs **6** in living mice over time. As shown in Figure 3, the main sites for accumulation of **6** are the urinary bladder and the liver after 5 min and 1 h post tail-vein injection. After 4 h, 24 h, and 48 h postinjection, $Si_{Mn}$ QDs **6** were found to mainly accumulate in the liver. Only a weak signal was seen in the bladder after 4 h postinjection.

The absolute quantification of biodistribution and deposition of $Si_{Mn}$ QDs **6** in living mice was obtained via gamma counting of *ex vivo* tissues. The four mice used for PET imaging were sacrificed after 48-h PET scan, and organs were harvested and analyzed quantitatively by a gamma-counter detector. The mean and SD of %ID/g have been corrected for natural decay of $^{64}Cu$. Liver was found to be the major organ where $Si_{Mn}$ QDs **6** accumulated (Figure 4). In detail, the liver accumulated 12.4 ± 1.0%ID/g of $Si_{Mn}$ QDs **6**, whereas the left and right kidneys took up 4.1 ± 1.3%ID/g and 3.0 ± 0.3%ID/g of **6**, respectively. Heart (4.2 ± 0.4%ID/g), intestine (3.8 ± 0.8%ID/g), spleen (2.4 ± 0.1%ID/g), and lung (2.2 ± 0.6%ID/g) also showed localization of $Si_{Mn}$ QDs **6**, and a small amount of **6** was found in the bladder (0.6 ± 0.5%ID/g) and brain (0.5 ± 0.1%ID/g).

Among many factors that may affect the biodistribution of systemically administered QDs in the body, the size of nanoparticles is critical.[30–33] Immediately upon exposure to blood, QDs may be quickly adsorbed by opsonins and in turn flagged for phagocytosis, an obligate response of the immune system when encountering a nanoparticulate foreign body.[30,34] Small nanoparticles (<7 nm) may be rapidly and efficiently eliminated via renal filtration with excretion into the urine, while larger particles are taken up nonspecifically by the reticuloendothelial system (RES) and end up in the liver, spleen, and lymphatic system, where they are excreted into the biliary system after hepatobiliary (HB) processing and enter

the gall bladder and intestine.[20,30,35–37] Our observations for biodistribution are consistent with expectations based on size (Figure 5). We conjecture that the fraction of $Si_{Mn}$ QDs **6** with small hydrodynamic diameter was rapidly excreted from the body through renal filtration and urinary bladder, while the fraction of $Si_{Mn}$ QDs **6** with larger hydrodynamic diameter was taken up by the RES and accumulated in the liver.

In conclusion, these results present the first analysis of *in vivo* biodistribution for Si QDs radiolabeled with a positron-emitting tracer. Knowledge of detailed biodistribution of QDs in living animals is of paramount importance before diagnostic or therapeutic application in the clinic is possible.[4,6,32] The present study shows rapid clearance of dextran coated Si QDs from mouse bloodstream, and the QDs were excreted from the body via both renal filtration and urinary bladder, and accumulated in the liver, which may provide useful information for the future design of new QDs and nanoparticles for biomedical applications.

## Supplementary Material

Refer to Web version on PubMed Central for supplementary material.

## Acknowledgments

The authors wish to acknowledge the National Institute of Health (HL081108-01 and EB008576-01) and the Center for Molecular and Genomic Imaging at the University of California, Davis (U24 CA 110804) for support of this work. We thank Tonya M. Atkins, Michelle Connell, and Jennifer Fung for their assistance with ICP-MS measurement and gamma counting.

## References

1. Ballou B, Lagerholm BC, Ernst LA, Bruchez MP, Waggoner AS. Noninvasive imaging of quantum dots in mice. Bioconjugate Chem. 2004; 15:79–86.
2. Allen PM, Liu WH, Chauhan VP, Lee J, Ting AY, Fukumura D, Jain RK, Bawendi MG. As(ZnCdS) Quantum Dots Optimized for Biological Imaging in the Near-Infrared. J Am Chem Soc. 2010; 132:470. [PubMed: 20025222]
3. Bentolila LA, Ebenstein Y, Weiss S. Quantum Dots for In Vivo Small-Animal Imaging. J Nucl Med. 2009; 50:493–496. [PubMed: 19289434]
4. Schipper ML, Cheng Z, Lee SW, Bentolila LA, Iyer G, Rao JH, Chen XY, Wul AM, Weiss S, Gambhirl SS. MicroPET-based biodistribution of quantum dots in living mice. J Nucl Med. 2007; 48:1511–1518. [PubMed: 17704240]
5. Pelley JL, Daar AS, Saner MA. State of Academic Knowledge on Toxicity and Biological Fate of Quantum Dots. Toxicol Sci. 2009; 112:276–296. [PubMed: 19684286]
6. Pic E, Bezdetnaya L, Guillemin F, Marchal F. Quantification Techniques and Biodistribution of Semiconductor Quantum Dots. Anti-Cancer Agents Med Chem. 2009; 9:295–303.
7. Warner JH, Hoshino A, Yamamoto K, Tilley RD. Water-soluble photoluminescent silicon quantum dots. Angew Chem, Int Ed. 2005; 44:4550–4554.
8. Zhang XM, Neiner D, Wang SZ, Louie AY, Kauzlarich SM. A new solution route to hydrogen-terminated silicon nanoparticles: synthesis, functionalization and water stability. Nanotechnology. 2007:18.
9. Erogbogbo F, Yong KT, Roy I, Xu GX, Prasad PN, Swihart MT. Biocompatible luminescent silicon quantum dots for imaging of cancer cells. ACS Nano. 2008; 2:873–878. [PubMed: 19206483]
10. Sudeep PK, Page Z, Emrick T. PEGylated silicon nanoparticles: synthesis and characterization. Chem Commun. 2008:6126–6127.
11. Tu CQ, Ma XC, Pantazis P, Kauzlarich SM, Louie AY. Paramagnetic, Silicon Quantum Dots for Magnetic Resonance and Two-Photon Imaging of Macrophages. J Am Chem Soc. 2010; 132:2016–2023. [PubMed: 20092250]

12. Cai WB, Shin DW, Chen K, Gheysens O, Cao QZ, Wang SX, Gambhir SS, Chen XY. Peptide-labeled near-infrared quantum dots for imaging tumor vasculature in living subjects. Nano Lett. 2006; 6:669–676. [PubMed: 16608262]
13. Lecoq P. Molecular Imaging Challenges With PET. IEEE Trans Nucl Sci. 2010; 57:1485–1491.
14. Shokeen M, Anderson CJ. Molecular Imaging of Cancer with Copper-64 Radiopharmaceuticals and Positron Emission Tomography (PET). Acc Chem Res. 2009; 42:832–841. [PubMed: 19530674]
15. Bengel FM, Higuchi T, Javadi MS, Lautamaki R. Cardiac Positron Emission Tomography. J Am Coll Cardiol. 2009; 54:1–15. [PubMed: 19555834]
16. Palko HA, Fung JY, Louie AY. Positron emission tomography: A novel technique for investigating the biodistribution and transport of nanoparticles. Inhalation Toxicology. 2010; 22:657–668. [PubMed: 20373851]
17. Jarrett BR, Gustafsson B, Kukis DL, Louie AY. Synthesis of Cu-64-labeled magnetic nanoparticles for multimodal imaging. Bioconjugate Chem. 2008; 19:1496–1504.
18. Gustafsson B, Youens S, Louie AY. Development of contrast agents targeted to macrophage scavenger receptors for MRI of vascular inflammation. Bioconjugate Chem. 2006; 17:538–547.
19. Cai WB, Chen K, Li ZB, Gambhir SS, Chen XY. Dual-function probe for PET and near-infrared fluorescence imaging of tumor vasculature. J Nucl Med. 2007; 48:1862–1870. [PubMed: 17942800]
20. Geraldes C, Laurent S. Classification and basic properties of contrast agents for magnetic resonance imaging. Contrast Media Mol Imaging. 2009; 4:1–23. [PubMed: 19156706]
21. Wadas TJ, Wong EH, Weisman GR, Anderson CJ. Coordinating Radiometals of Copper, Gallium, Indium, Yttrium, and Zirconium for PET and SPECT Imaging of Disease. Chem Rev. 2010; 110:2858–2902. [PubMed: 20415480]
22. Anderegg G, Arnaud-Neu F, Delgado R, Felcman J, Popov K. Critical evaluation of stability constants of metal complexes of complexones for biomedical and environmental applications. Pure Appl Chem. 2005; 77:1445–1495.
23. Glaus C, Rossin R, Welch MJ, Bao G. In Vivo Evaluation of Cu-64-Labeled Magnetic Nanoparticles as a Dual-Modality PET/MR Imaging Agent. Bioconjugate Chem. 2010; 21:715–722.
24. Li WP, Meyer LA, Capretto DA, Sherman CD, Anderson CJ. Receptor-binding, biodistribution, and metabolism studies of Cu-64-DOTA-cetuximab, a PET-imaging agent for epidermal growth-factor receptor-positive tumors. Cancer Biother Radiopharm. 2008; 23:158–171. [PubMed: 18454685]
25. Duimstra JA, Femia FJ, Meade TJ. A gadolinium chelate for detection of beta-glucuronidase: A self-immolative approach. J Am Chem Soc. 2005; 127:12847–12855. [PubMed: 16159278]
26. Wangler C, Wangler B, Eisenhut M, Haberkorn U, Mier W. Improved syntheses and applicability of different DOTA building blocks for multiply derivatized scaffolds. Bioorg Med Chem. 2008; 16:2606–2616. [PubMed: 18065226]
27. Herman S, Persijn G, Vandekerckhove J, Schacht E. Synthesis of dextran derivatives with thiol-specific reactive groups for the preparation of dextran protein conjugates. Bioconjugate Chem. 1993; 4:402–405.
28. Li YL, Zhu L, Liu ZZ, Cheng R, Meng FH, Cui JH, Ji SJ, Zhong ZY. Reversibly Stabilized Multifunctional Dextran Nanoparticles Efficiently Deliver Doxorubicin into the Nuclei of Cancer Cells. Angew Chem, Int Ed. 2009; 48:9914–9918.
29. Jones-Wilson TM, Deal KA, Anderson CJ, McCarthy DW, Kovacs Z, Motekaitis RJ, Sherry AD, Martell AE, Welch MJ. The in vivo behavior of copper-64-labeled azamacrocyclic complexes. Nucl Med Biol. 1998; 25:523–530. [PubMed: 9751418]
30. Smith AM, Duan HW, Mohs AM, Nie SM. Bioconjugated quantum dots for in vivo molecular and cellular imaging. Adv Drug Delivery Rev. 2008; 60:1226–1240.
31. Alexis F, Pridgen E, Molnar LK, Farokhzad OC. Factors affecting the clearance and biodistribution of polymeric nanoparticles. Mol Pharmaceutics. 2008; 5:505–515.
32. Choi HS, Liu W, Misra P, Tanaka E, Zimmer JP, Ipe BI, Bawendi MG, Frangioni JV. Renal clearance of quantum dots. Nat Biotechnol. 2007; 25:1165–1170. [PubMed: 17891134]

33. Balogh L, Nigavekar SS, Nair BM, Lesniak W, Zhang C, Sung LY, Kariapper MST, El-Jawahri A, Llanes M, Bolton B, Mamou F, Tan W, Hutson A, Minc L, Khan MK. Significant effect of size on the in vivo biodistribution of gold composite nanodevices in mouse tumor models. Nanomed-Nanotechnol Biol Med. 2007; 3:281–296.

34. Owens DE, Peppas NA. Opsonization, biodistribution, and pharmacokinetics of polymeric nanoparticles. Int J Pharm. 2006; 307:93–102. [PubMed: 16303268]

35. Longmire M, Choyke PL, Kobayashi H. Clearance properties of nano-sized particles and molecules as imaging agents: considerations and caveats. Nanomedicine. 2008; 3:703–717. [PubMed: 18817471]

36. Aime S, Caravan P. Biodistribution of Gadolinium-Based Contrast Agents, Including Gadolinium Deposition. J Magn Reson Imaging. 2009; 30:1259–1267. [PubMed: 19938038]

37. Bimbo LM, Sarparanta M, Santos HA, Airaksinen AJ, Makila E, Laaksonen T, Peltonen L, Lehto VP, Hirvonen J, Salonen J. Biocompatibility of Thermally Hydrocarbonized Porous Silicon Nanoparticles and their Biodistribution in Rats. ACS Nano. 2010; 4:3023–3032. [PubMed: 20509673]

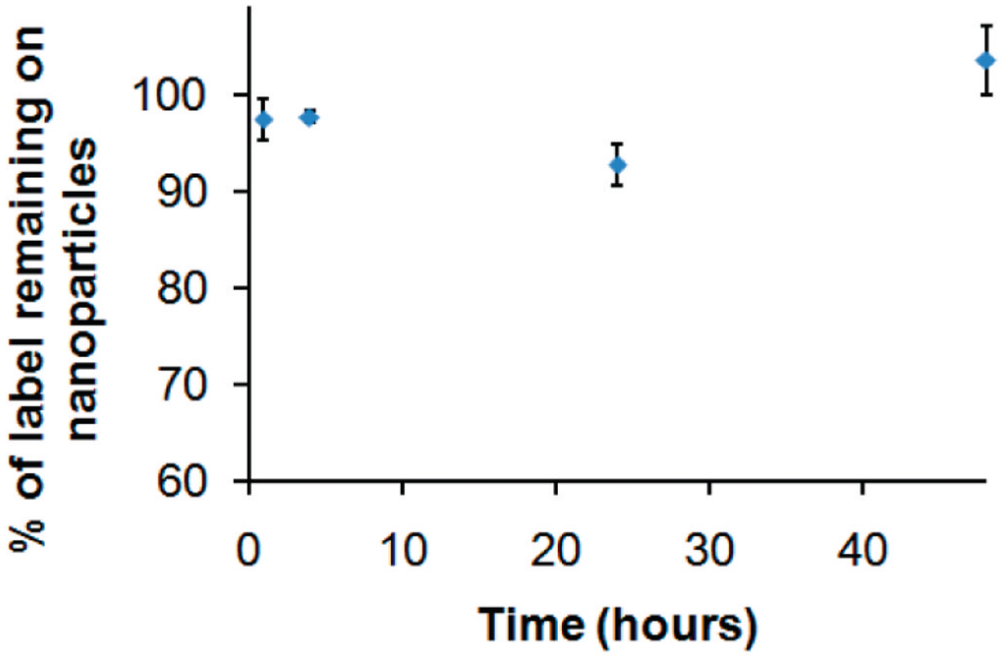


**Figure 1.**
Stability of QDs **6**-$^{64}$Cu in pH 5.5 sodium acetate–acetic acid buffer solution over the 48 h time period.

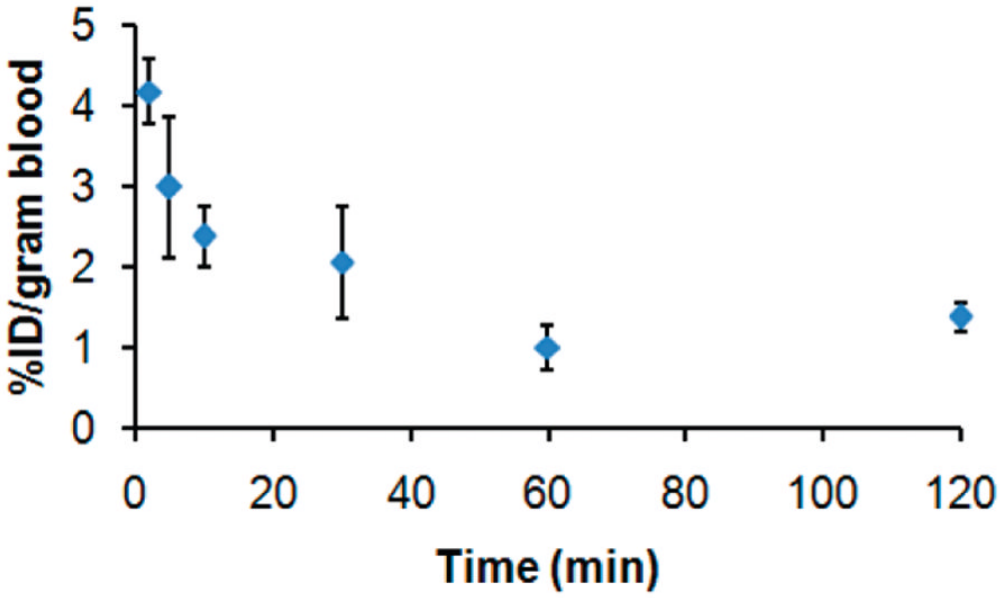


**Figure 2.**
Blood clearance of $^{64}$Cu-DO3A conjugated dextran $Si_{Mn}$ QDs **6** in mice ($n$ = 3).

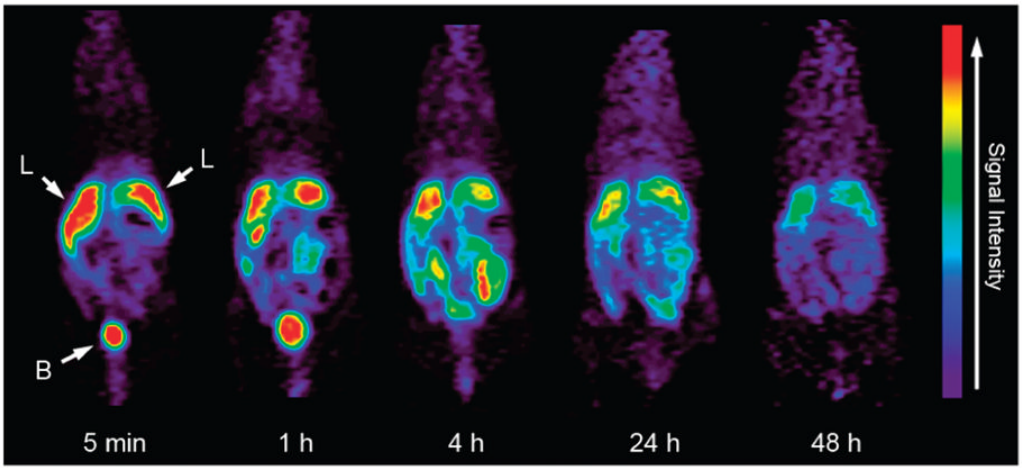


**Figure 3.**
*In vivo* PET images of mice ($n$ = 4) at 5 min, 1 h, 4 h, 24 h, and 48 h postinjection of $^{64}$Cu-DO3A conjugated dextran $Si_{Mn}$ QDs **6**: L, liver; B, bladder.

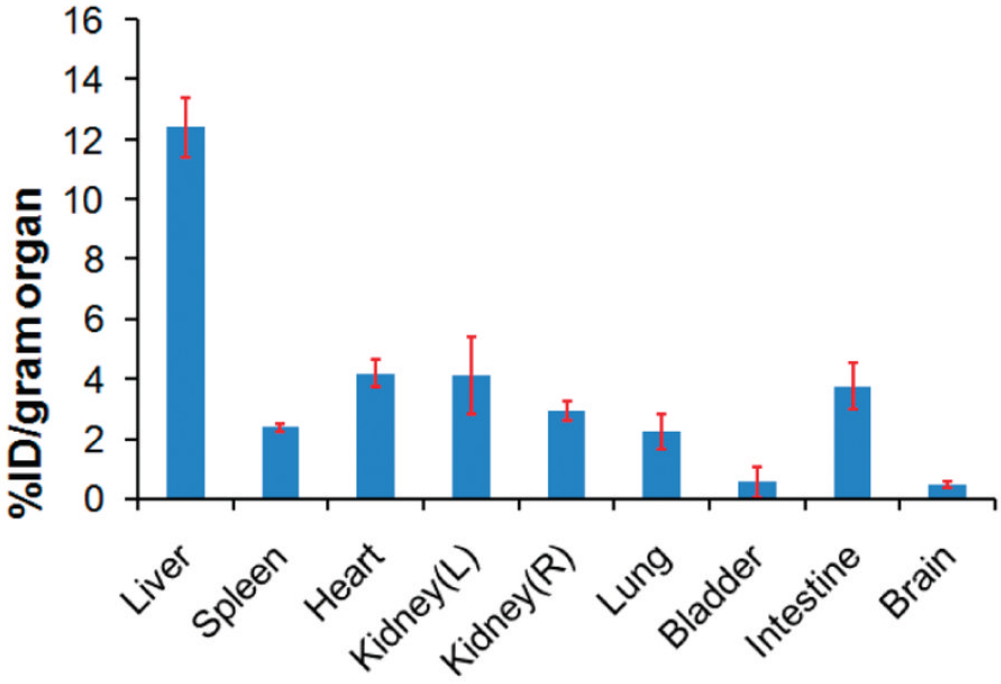


**Figure 4.**

*Ex vivo* biodistribution of $^{64}$Cu-DO3A conjugated dextran $Si_{Mn}$ QDs **6** in mice. Mice ($n$ = 4) were sacrificed 48 h post intravenous injection. Organs were harvested and measured by well gamma counting.

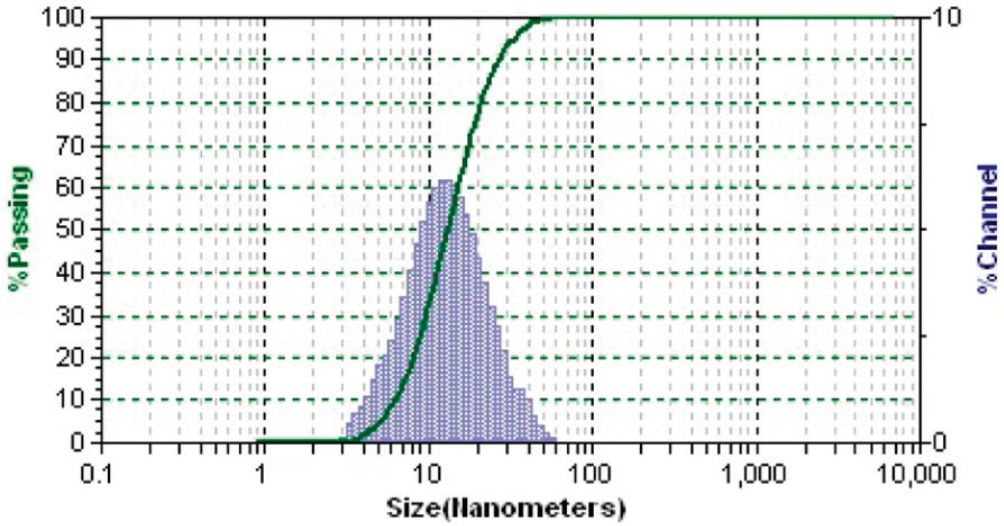


**Figure 5.**
Hydrodynamic diameter of DO3A conjugated dextran $Si_{Mn}$ QDs **5** measured by dynamic light scattering (DLS).

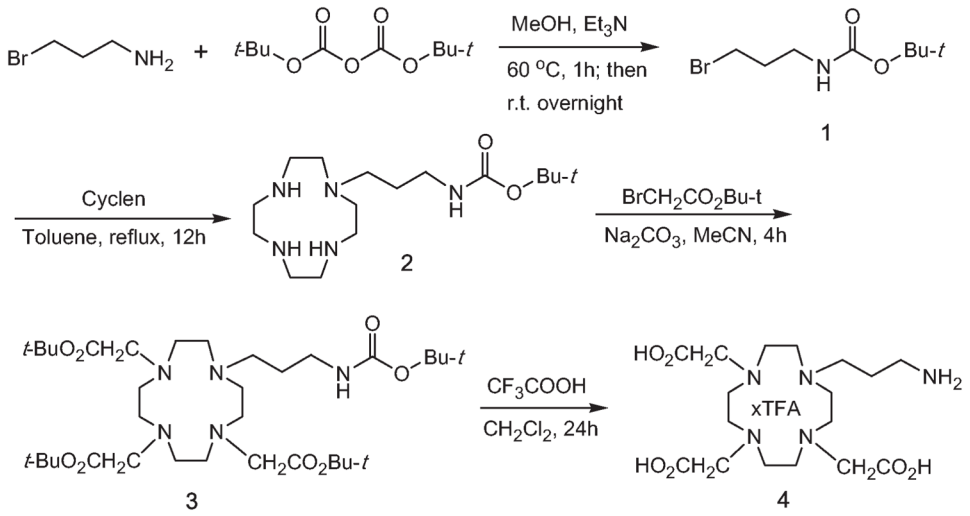


**Scheme 1.**
Synthesis of Ligand 4 for $^{64}$Cu Chelation

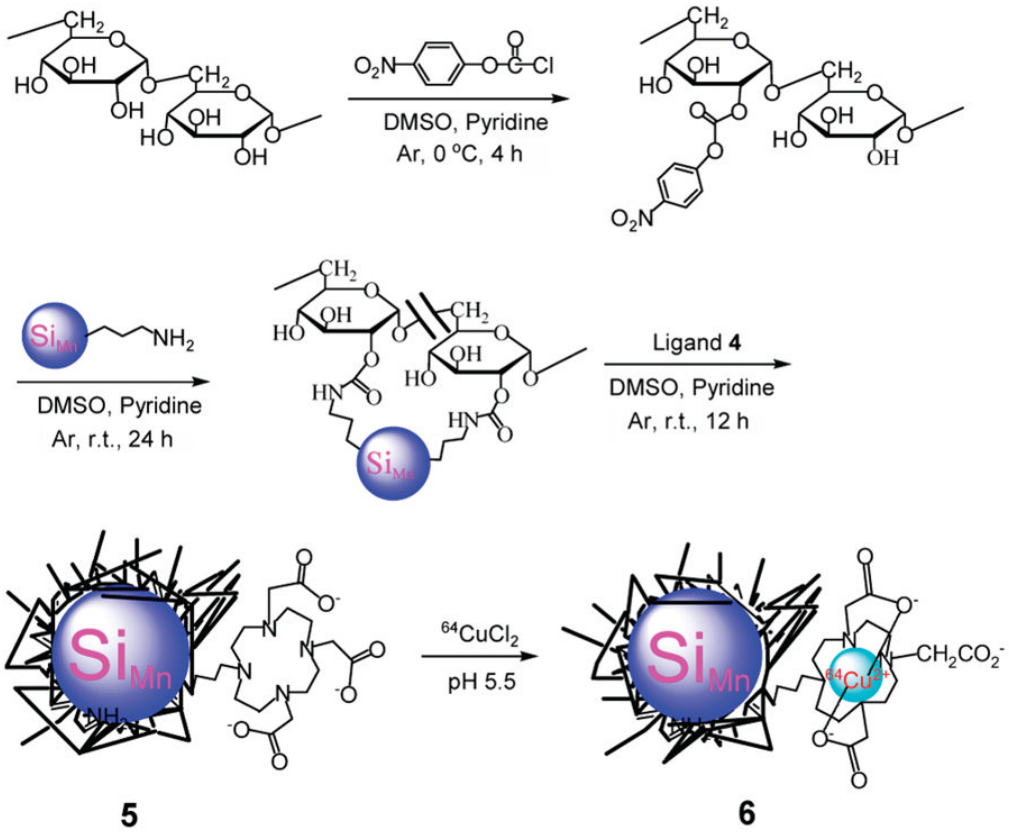


**Scheme 2.**
Synthesis of $^{64}$Cu-DO3A Conjugated Dextran $Si_{Mn}$ QDs 6